Laetoli Footprint model results

August 18, 2020

Lawrence B. Conyers

A model of the Laetoli footprints in Tanzania (Figure 1) was created in July, 2020 in order to simulate what the prints would look like, and to test a variety of GPR acquisition methods and processing techniques to image them. Published information on some of the prints was used to determine the depth necessary in the model (Figure 2).

Figure 1: The exposed Laetoli prints in Tanzania that are about 3.2 million years old.

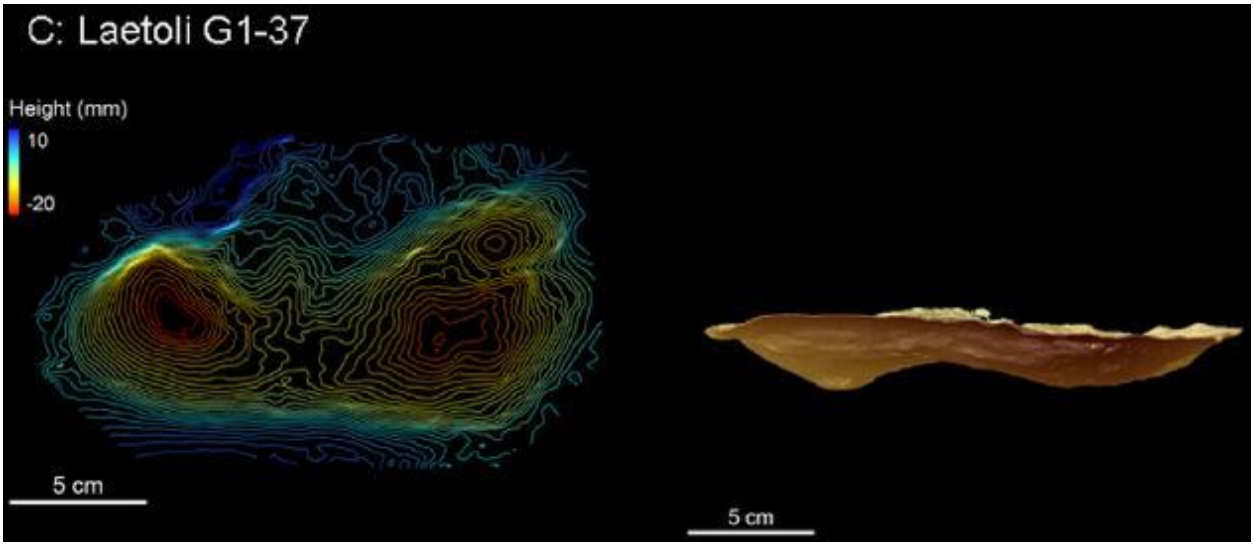

Figure 2: detailed 3-D analysis of one of the Laetoli prints (from Raichlen et al. 2010) that was mimicked in the model

Production of the model

This model was created in Oregon on level ground consisting of basaltic weathered clay. The surface was cleared of vegetation and watered down for three hours to create a muddy surface. That surface was further raked and leveled by hand to mimic the lake bottom as was exposed at Laetoli (Figure 3). The grid was 180x 100 cm in dimension, with the long axis east-west.

Figure 3: Creation of the footprint model in Oregon, with the boards outlining the test grid that was 180x100 cm in dimension.

Two sets of prints were then produced in the wet clay, one “male” and one “female”. The male prints were created by Larry Conyers and the female prints by Rachel Leo. The depth of the prints ranged from 1.5-2.8 cm depth, consistent with the measured depth of the prints from Laetoli (Raichlen et al. 2010). The stride (distance between steps) was much less than at Laetoli to place 12 prints into the model area. Some of the prints had very good imprints of toes and heels, while others were less distinct (Figure 4), which was done on purpose to create a variety of shapes and depths. The model was then sun-dried for a day in very hot weather.

Figure 4: Creating the print model in Oregon

Figure 4: Differences in footprints created in the model.

The model was then covered by a sheet of plywood with a void space between the top of the clay and the base of the plywood sheet of about 10-12 cm. The wood was gridded with lines every 10 cm, along which the antennas were moved (Figure 5).

Figure 5: Covering the model with plywood.

Reflection data collection

The GSSI SIR-3000 system was used with 900, 2000 and 2600 MHz antennas. Data were collected in a time window of 8 ns with 512 samples/trace and between 400 and 800 traces/meter. Lines were all collected 10 cm apart, except for one small grid that has a 5 cm line spacing.

Reflection profiles were first collected both north-south and east-west on the plywood surface using the 2.6 GHZ antenna (Figure 6).

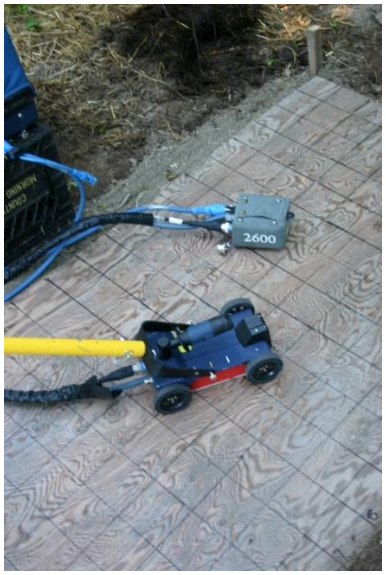

Figure 6: The 2.6 GHZ antenna used on the plywood surface.

The 2.6 GHZ reflection profiles are quite good at imaging the clay layer, but variations in the plywood created distortions in the reflections (Figure 7) that tended to destroy the continuity of the clay reflection along the length of the profile.

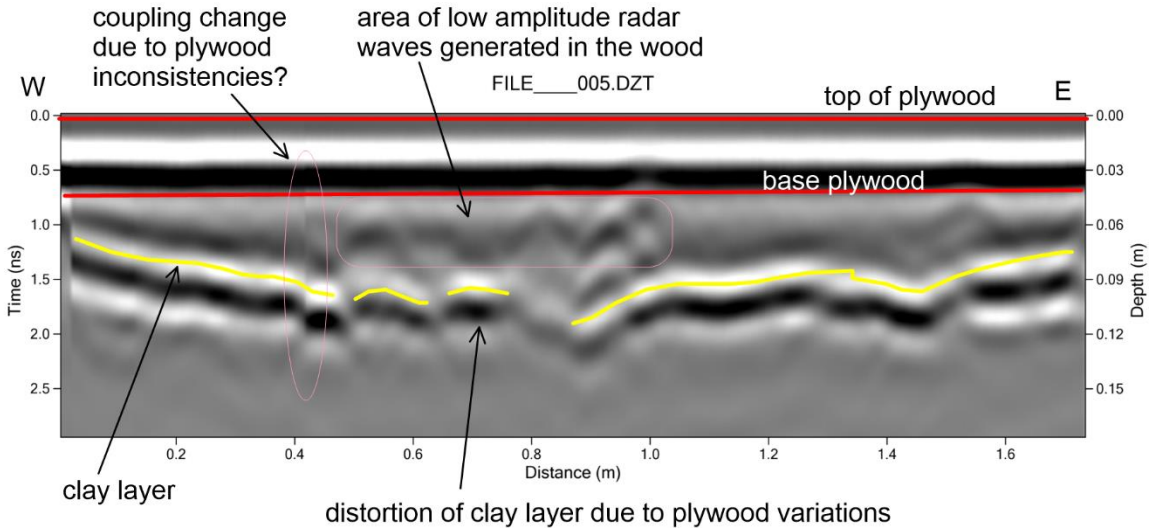

Figure 7: Reflection profile using the 2.6 GHz antenna showing the distortions in the clay layer due to variations in the plywood.

The 900 MHz antenna was then used on this surface and the reflection profiles from it were found to be very poor (Figure 8). While there is a hint of the clay surface, there is not enough resolution to be able to do anything whatever with defining the footprints using this antenna.

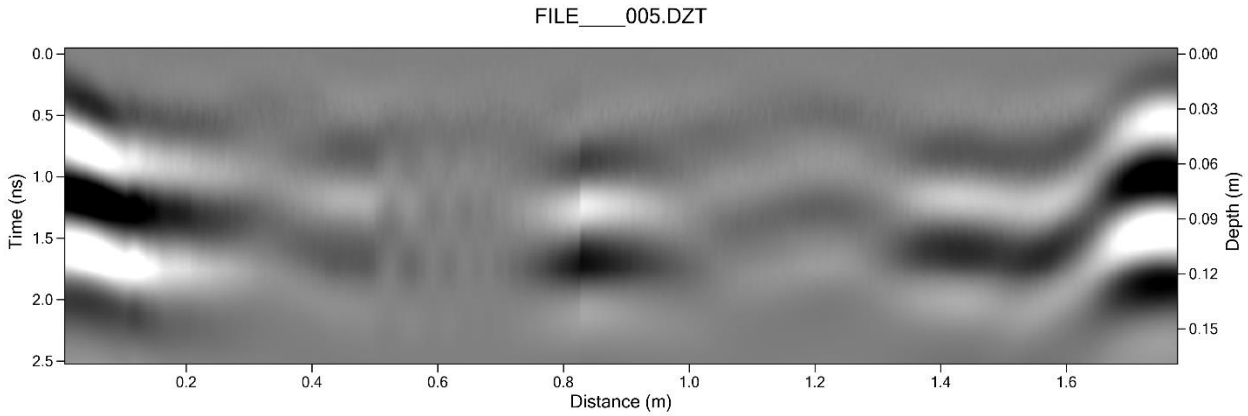

Figure 8: 900 MHz antenna reflection profile on the plywood.

While the plywood test was marginally suitable for imaging the footprints, it was decided that there is too much error being generated by variations in the plywood. Also, the energy that is transmitted through the plywood and then moved in air before encountering the clay spread out too much, and this conical spreading also reduced the resolution of the clay bed reflection (Conyers 2013).

The clay model was then covered with basalt sand, imported from a nearby quarry. All prints were first filled individually with sand, and then the whole model area was buried in 5.5-6.5 cm of sand. The sand surface was then leveled (Figure 9).

Figure 9: Covering the model with basalt sand

While placing the plywood on the sand improved the quality of the 2.6 GHz reflections somewhat, there was still a good deal of distortion due to plywood inconsistencies (Figure 10).

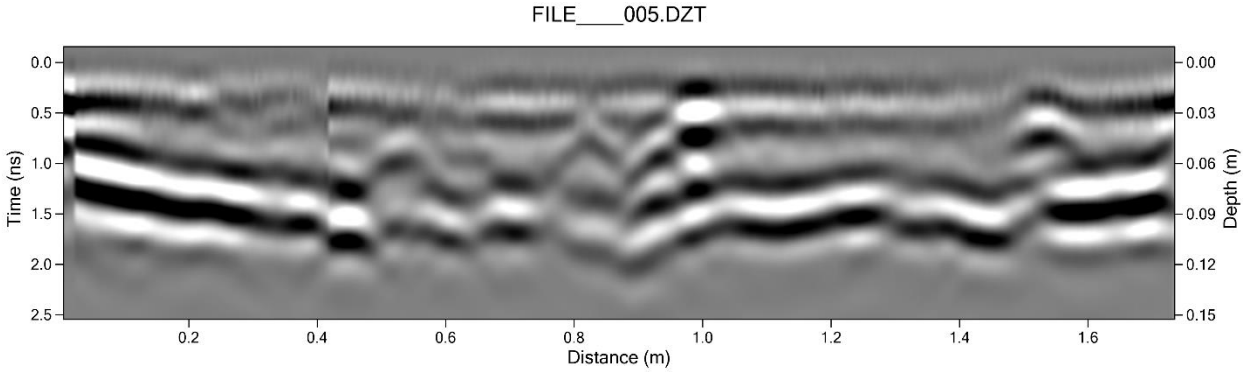

Figure 10: 2.6 GHz reflection profile showing the same distortions due to plywood inconsistencies.

These distortions caused by the plywood may be related to air pockets below the plywood, caused by an uneven sand surface. To test whether this was the case a ¼ inch (8 mm) thick “yoga mat” (Figure 11) made of poly-vinyl-chloride plastic (PCV) was then placed on the sand (Figure 11) and gently pushed down to fill in any air pockets.

Figure 10: PVC yoga mat ¼ inch thick (8 mm) used to cover the sand

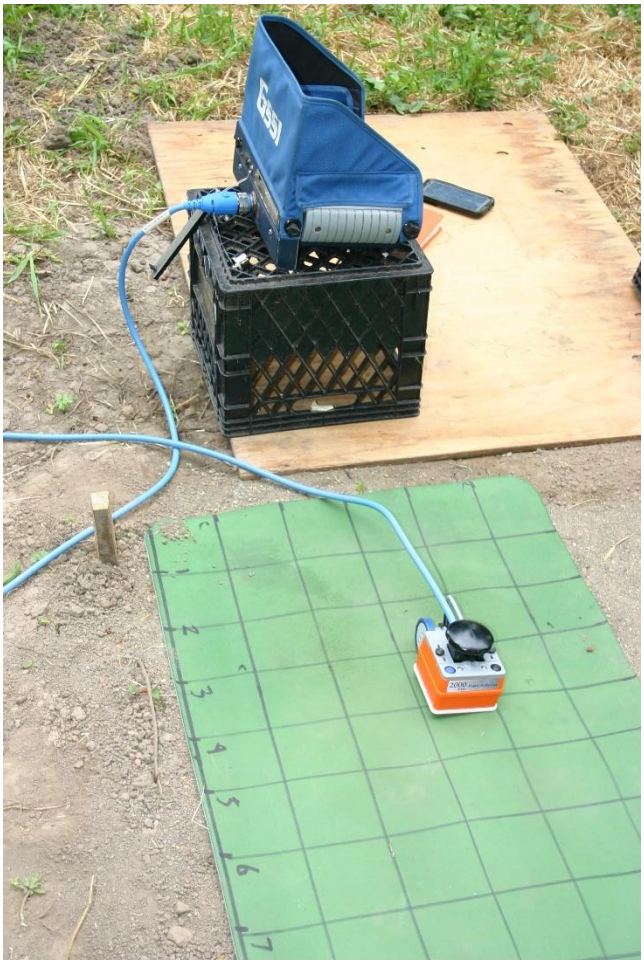

Figure 11: Yoga map that was gridded in the same way as the plywood surface. This mat filled in the minor undulations in the sand surface, removing any air pockets that were present. The antenna here is the 2 GHz palm antenna.

This was a much better surface for collecting GPR data, as the variations in the plywood were removed (Figure 12). However, minor air pockets below the PVC mat still produced extraneous reflections. These profiles were much better than all the methods used prior to this and may be a more accurate model for what data might be like collected over uneven ground at Laetoli. The air pockets may be creating error in this method that can't be removed. The clay surface is much more continuous and distinct using the

PVC yoga mat over the sand. As will be shown below, this method produced very good results for imaging the model prints. All further tests used only the 2.6 GHz antennas.

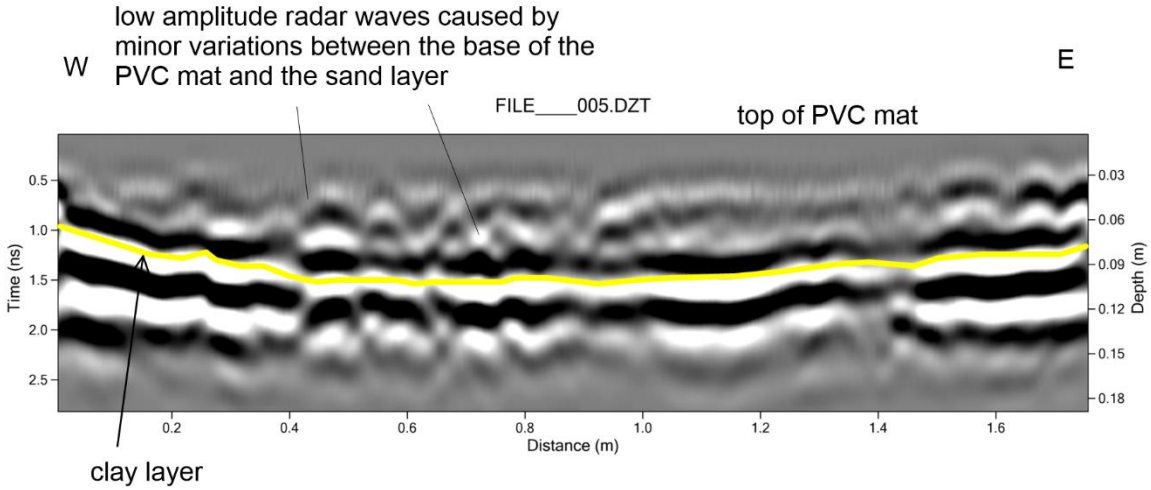

Figure 12: Reflection profile using the 2.6 GHz antenna on the PVC mat placed directly on the sand.

One additional method was also tried here, using the 2 GHz antenna (shown in Figure 11). This "palm" antenna is typically used for concrete evaluations and proved to be inferior in all respects to the 2.6 GHz. I am not exactly sure why this is, but the reflection profiles from the 2 GHz tended to produce multiples of the clay surface below the initial reflections. I noticed during collection that this antenna tended to "stick" to the PVC mat surface also, perhaps producing the dramatic variations on the clay reflection surface.

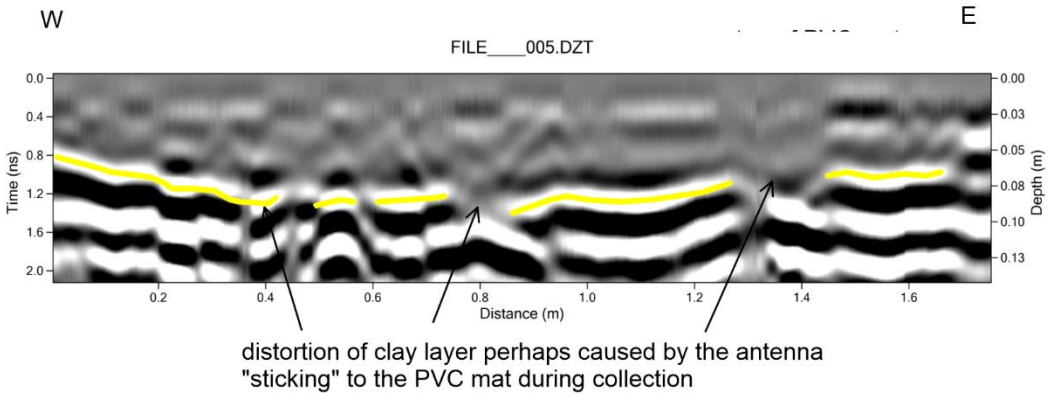

Figure 13: 2 GHz palm antenna reflection profile collected on the PVC mat.

Interpretation of results

The 900 MHz and 2 GHZ reflection data were not used in the following interpretation. The 2.6 GHz antenna was superior in all respects to the other antennas, and the "yoga mat" or PVC covering also produced the most coherent reflections of the clay layer with the prints, covered by sand. Those methods and antenna data are used in the following analysis.

A two-dimensional model of the prints below the sand layer was then created to which all results were compared (Figure 14).

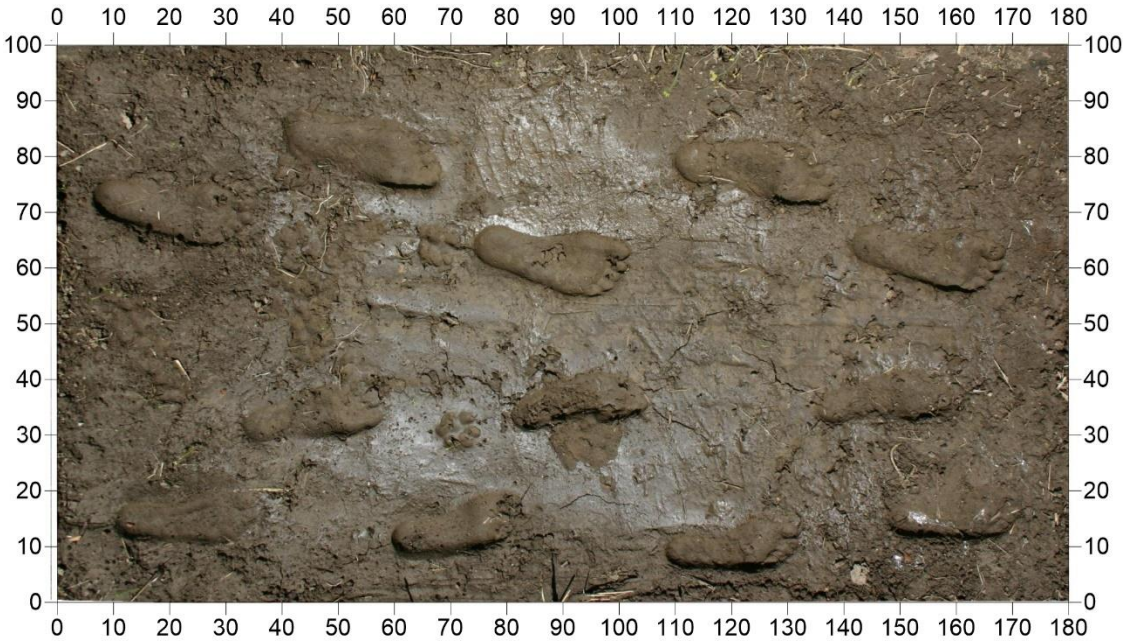

Figure 14: The footprint model.

It was quickly determined that toes of the prints were impossible to image, so general outlines of he prints were outlined for comparison (Figure 15).

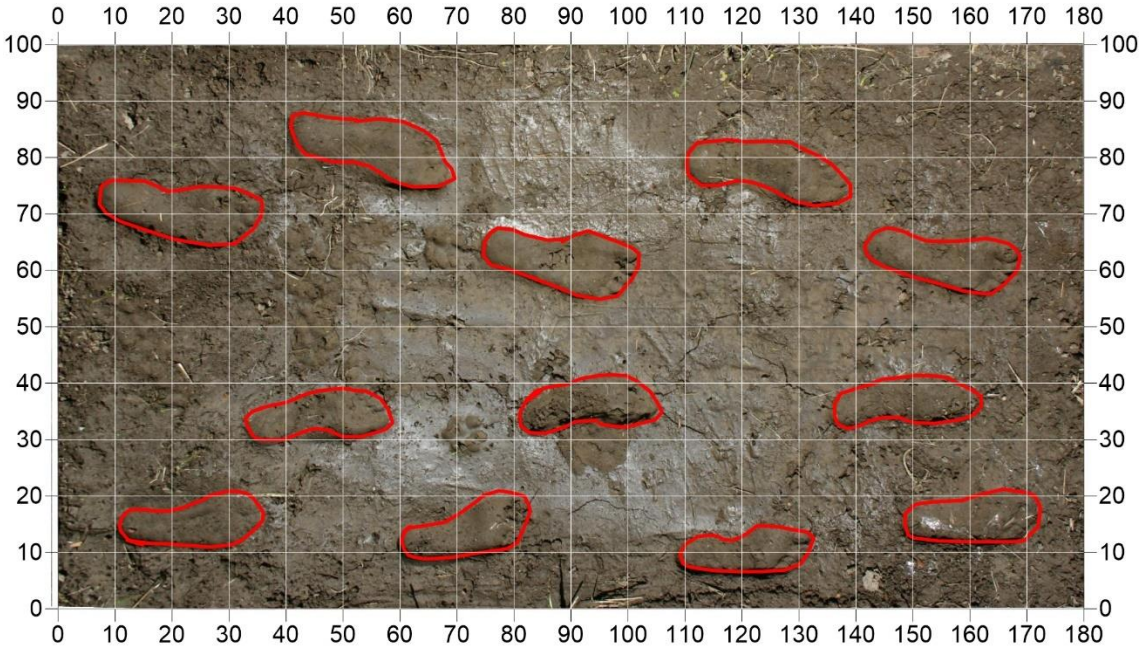

Figure 15: Print outlines used for comparison. The reflection profile locations are shown in white every 10 cm.

The first method employed was to create an amplitude map of the top of the clay layer to about .5 nanoseconds (ns) below it (about a 3 cm thick slice using an RDP of 5). In this way reflection features

that might be produced by differences in the amplitude of recorded reflection from the prints might show up (Figure 16).

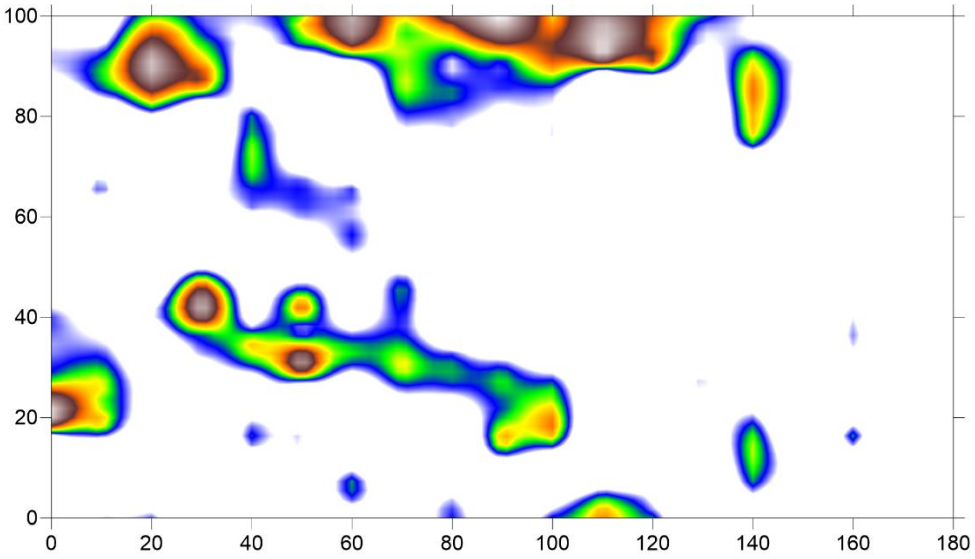

Figure 16: Reflection amplitude map showing different in the strength of the reflected waves generated from the clay layer on which the footprints were preserved. This is a 3 cm thick slice or .5 ns in two-way travel time.

These reflection features visible in Figure 16 were then placed on the model (Figure 17). In this comparison the general location of the high amplitude reflections has almost no spatial correlation to the prints. This was very disappointing.

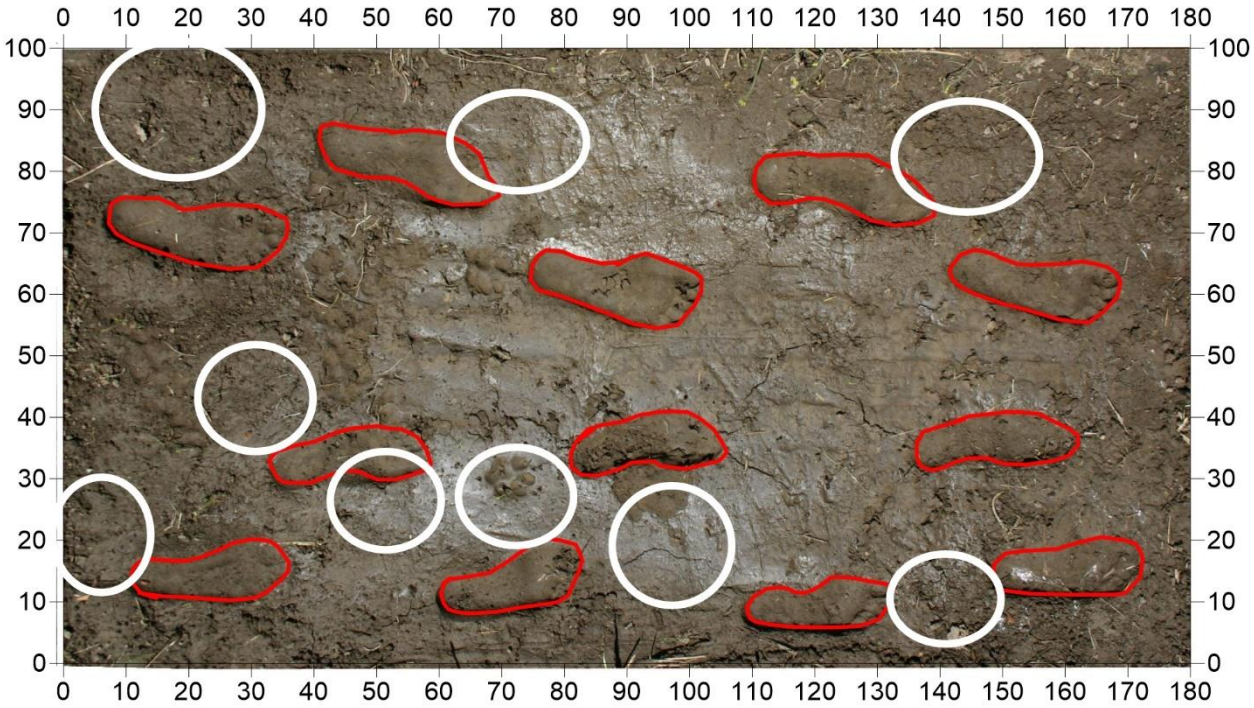

Figure 17: Reflection features compared to the prints. There is no correlation whatever.

The standard amplitude slice-map method used by so many as the tool for imaging the ground was totally ineffective here. It is likely that it is producing an image of differences in the sand composition or retained water in the sand that was used to fill in the prints.

As I have so often commented on (and rarely listened to by the GPR community), GPR analysis without a detailed analysis of the two-dimensional reflection profile interpretation is leaving about 95% or more of the data un-used (Conyers 2016; Conyers et al. 2019). Using reflection profile analysis, I then went through each profile individually and looked for depressions in the clay layer that correspond to the known prints. All possible prints visible in the profiles were then given a unique x and y location within the test grid.

Two distinct types of print reflections were visible in the profiles (Figure 18). One of them is visible by a slight depression in the clay layer that produces a reflection hyperbola below. This is common in GPR and has been colloquially referred to as a "vertical bow tie" reflection (Conyers 2013). Elsewhere using much lower frequency antennas, I have seen these produced from canals and house floor depressions (Conyers 2012; 2013), but of course on a much larger scale than the project here. The hyperbolas below the print depression are produced by the spreading radar energy that moves through the ground in front of the antenna where it is then reflected off the farther edge of the print depression. The same is created as energy moves backward from the antenna and is reflected off the edge of the print after the antenna has already moved beyond that buried surface. The result is a hyperbola recorded below the footprint (Conyers 2012:166). A second type of footprint reflection is created when the print does not have as distinct an edge but is just a simple depression. In this case the concave upward surface of the print (probably the ball of the foot and the heel depressions) focuses radar energy that would otherwise be spreading out as it travels in the ground. That focused energy creates a higher amplitude reflection directly along the clay surface reflection. This has been defined elsewhere with GPR in much larger features than these prints, but the concept is the same (Conyers 2013: 72). In both cases the subtle depression of the print is visible (Figure 18).

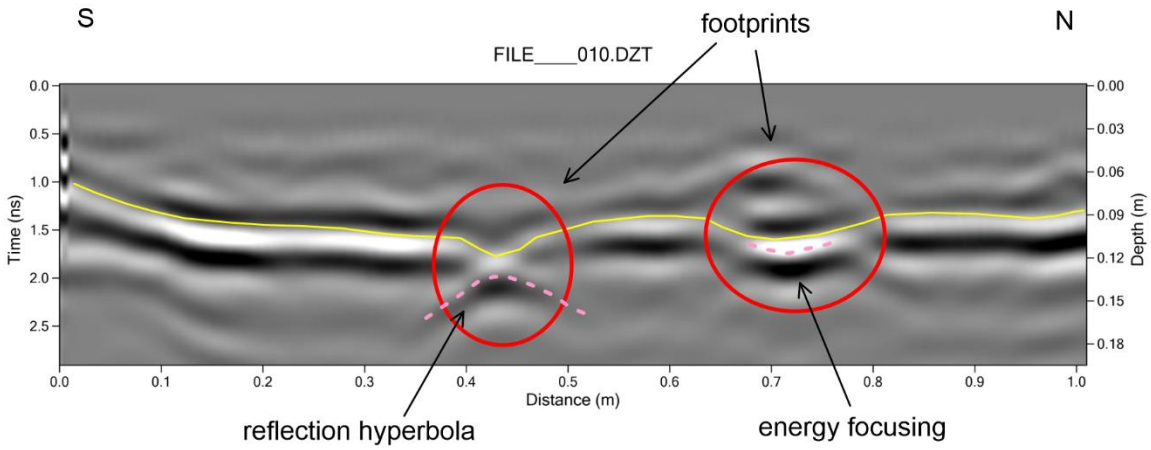

Figure 18: 2.6 GHz reflection profile showing two types of footprint reflection types.

In some profiles both reflection types are visible (both the creation or hyperbolas and the focusing of energy (Figure 19).

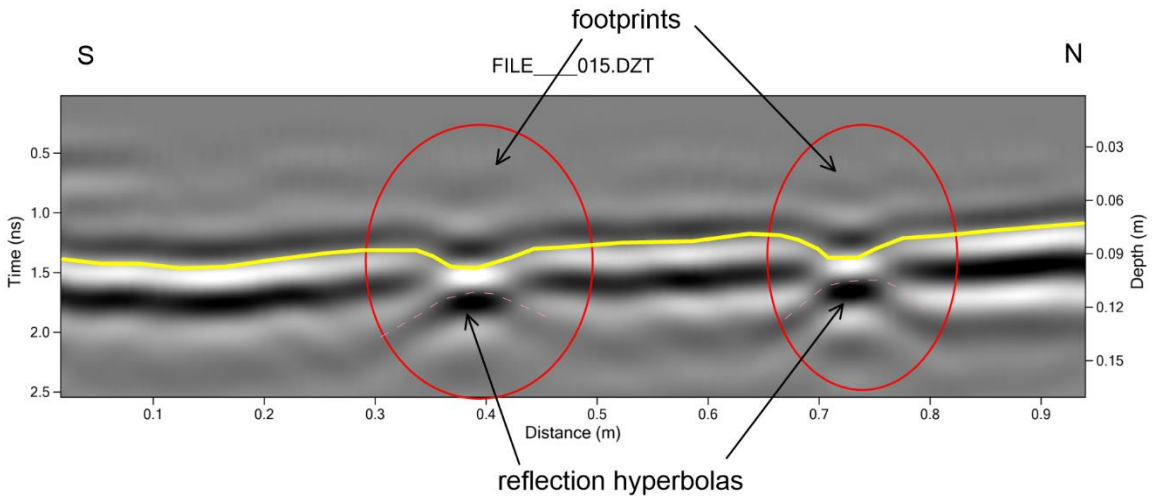

Figure 19: Two types of reflection types found together: hyperbolas and focusing from the base of the prints).

In reflection profiles that do not cross the prints neither of these reflection types are visible (Figure 20). Care must be taken in interpretation of profiles as coupling changed due to operator error or air pockets below the PVC mat were also found to create features that appear to be like some of the reflection variations of interest.

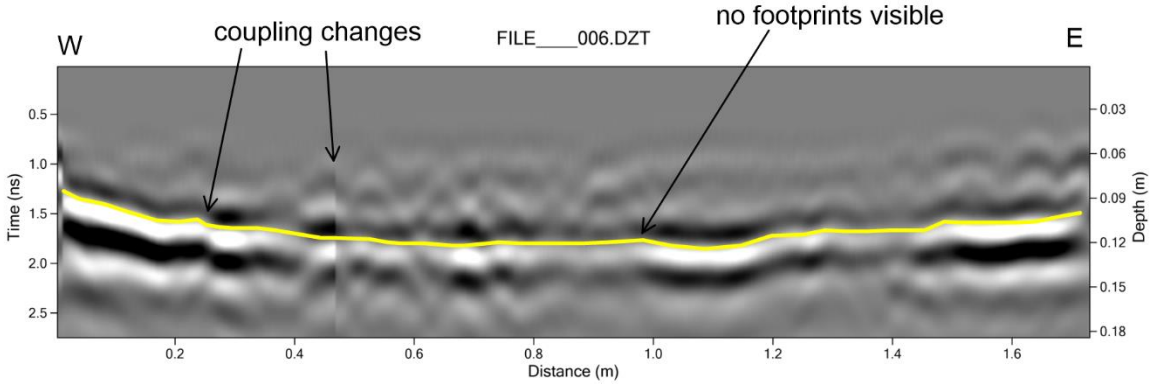

Figure 20: Reflection profile showing no footprint features but coupling changes.

All reflections that were of these two types (reflection hyperbolas and energy focusing) were then given locations in the grids. The middle of the features only was given these x and y locations. Those locations were then placed on top of the photo of the footprints (Figure 21). When this was done there was only one print that produced neither of these features described above. It must be so shallow or have no sides and therefore it can't reflect from its edges or has no ability to focus energy. In all the other cases it is the print edges, or the deeper part of the prints that is reflecting the energy (the heel or the ball of the foot). Three false positives were also identified using this visual method, which are close to the prints but not directly on them. In those profiles there may have been some antenna wheel slippage that created a distance error of about 8-9 cm. In these cases, I must have moved the antennas poorly or the attached encoder wheel was not directly in contact with the PVC mat. Other variations in the locations plotted may have been caused by radar energy moving at an sideways angle from the PVC mat to and from the prints not directly below the antenna, producing some distortion in the plotting of

the print reflections. This shows how important it is to spend a great deal of time in collection, especially when only a few centimeters in error can cause a good deal of error.

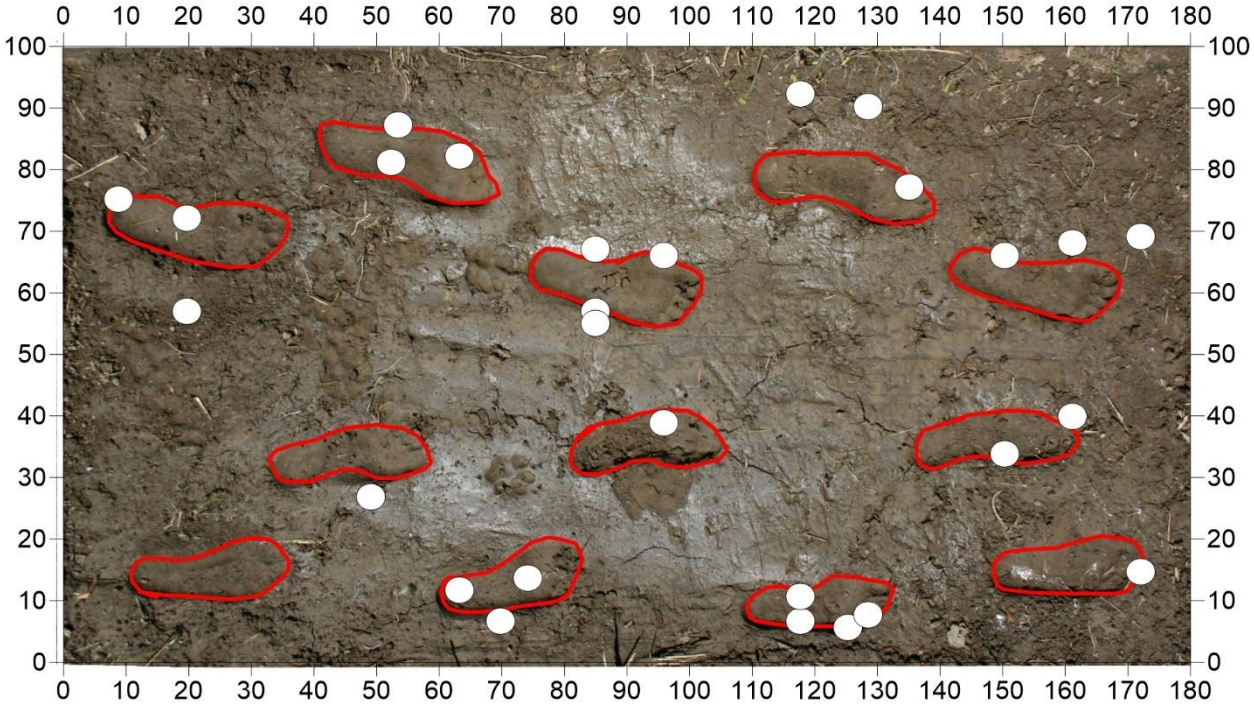

Figure 21: Locations of the reflections visible in individual profiles placed on the footprint image.

While the manual interpretation method looking for small undulations in the clay, often with associated reflection hyperbolas and energy focusing is a good way to define these features, a more "automated" ways to process data and produce images was still a priority. In the manual method (Figure 21) only one of the prints could not be identified (that in the southwest corner). There were two "false positives" for unknown reasons, and one print whose reflection signature was a few centimeters off the actual print location. That is a 75% success rate, with either 3 or 4 "near misses" and one total failure.

A method was then used termed "horizon slicing", which I have tried a few times, with limited success (Conyers and Goodman, 1997: 172). This method takes specialized software. I used ReflexW two-dimensional package (https://www.sandmeier-geo.de/reflex2dquick.html), but I know that GPR Slice (https://www.gpr-survey.com/) and RADAN (https://www.geophysical.com/software have similar data collection packages. The method allows a user to view each reflection profile individually, "pick" a horizon that is of interest, and then the software "follows" that horizon (usually following one wave phase along the profile). If the automatic picking "goes astray" one can go back and correct mistakes visually. This type of editing is common using this somewhat laborious method. One can then choose to save information about that horizon as an ASCII file, which can be manipulated by other programs such as Excel. I used that program to manipulate the digital data, and then Surfer (https://www.goldensoftware.com/products/surfer to produce the maps.

I found ReflexW to be quite difficult to use and not nearly as intuitive as I am used to in other software packages. For instance, I found it quite difficult to take individual profiles and process them in a way that would allow for the clay horizon to be visible in this software. Therefore, I first opened all the files

in my own software GPR Viewer (http://www.gpr-archaeology.com/software/) and processed them by removing background and gaining them appropriately (Figure 22). Those I then saved for processing later in ReflexW. The example in Figure 22 is one profile that crosses two of the prints. The clay horizon is visible at 1 nanosecond depth, and the prints display both reflection hyperbolas and energy focusing. The gain curve that was applied in GPR Viewer is on the right.

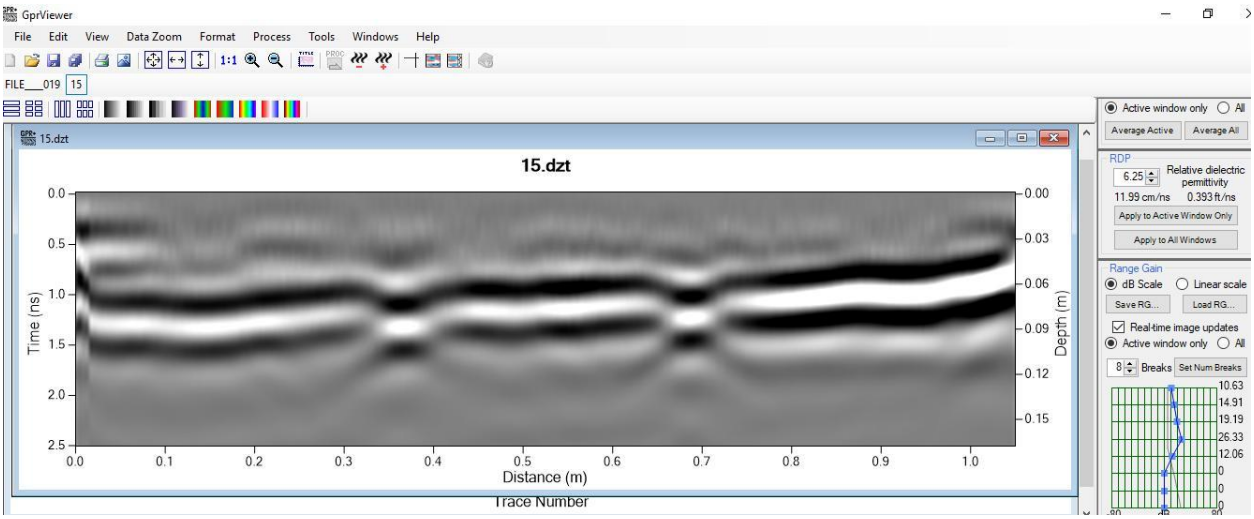

Figure 22: How profiles were first processed in GPR Viewer before being save for further analysis using ReflexW.

Those processed profiles were then imported into ReflexW and the clay horizon was visible and could be "picked" and "followed" easily (Figure 23) using the horizon slicing method. This was done for each of the 2.6 GHz profiles in the "yoga mat on sand" grid). It was immediately apparent in this operation that there was spatial error in the dataset, likely produced by slippage of the survey wheel attached to the antenna. For instance, in Figure 22 a 100 cm ling profile is displayed as 110 cm in length). I didn't notice this immediately during data collection and am unsure what caused these errors. Perhaps it was a the survey wheel calibration error I used prior to collection, or there was something about my method of moving the antenna that caused this slippage. I know that I placed a piece of plywood adjacent to the yoga mat that had the grid drawn on it. Perhaps the wheel rolled differently on the wood than the mat? Or was the small angle that the plywood was placed at enough to create this error? Or was I just sloppy in collection and neglected to start and stop the antenna at the correct locations in the grid? It could have been all these error-creating problems. This tells me that a great deal of attention must be paid to all aspects of collection when doing a project that necessitates this precision.

In addition to the distance error that I discovered, there were other errors that could not have been anticipated such as the variations in the amount of water and the grain size of the sand that was placed on the prints. I also found that during collection I had to kneel on the yoga mat, which tended to depress it in some places, creating a minor amount of undulation in the mat surface. At the time I didn't think this would cause much error, but now in hindsight I think it could have. There were also significant coupling errors at the start and end of each profile, caused by the antenna moving from the plywood to the yoga mat. Those were not "picked" in the horizon slicing method, and so some of the lines were shorter or longer than others. I also discovered that ReflexW only saves one digital point for each of the

traces that were collected. Here is calibrated the system to collect 400 traces per meter. I think that in the future twice that number would have been better, to produce a higher resolution.

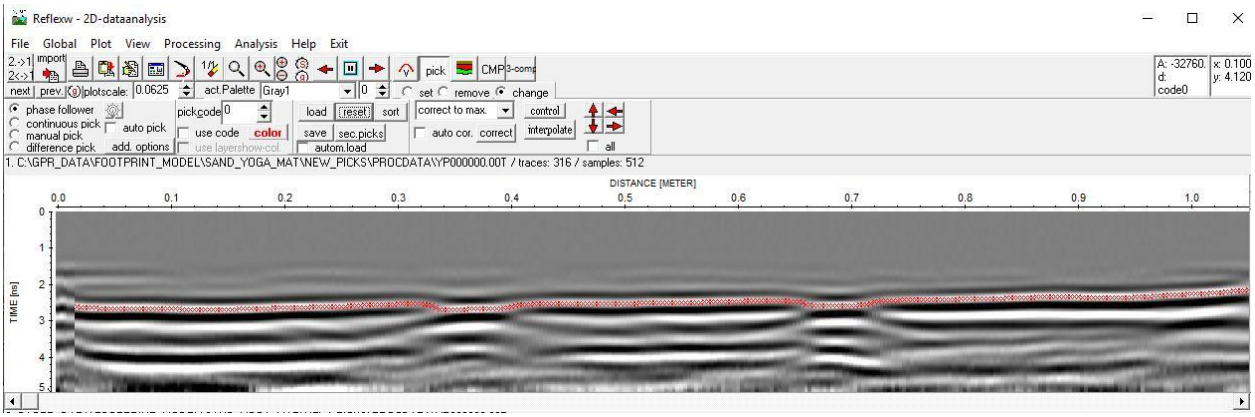

Figure 23: Picking the clay horizon in ReflexW from which the data were then saved.

In this test all the profiles were picked, and the data saved. The distinctive profile in Figure 22 is displayed in Figure 24 showing the GPR Viewer image at the top and then the saved "picks" for depth below and the reflection wave amplitudes at the bottom. This is very interesting as it shows how precise the ReflexW software is in obtaining depth, and those values show the prints very well in a profile. The amplitudes, which are also saved in this process along with depth, were plotted, and they display the energy focusing from the base of the prints as a small increase in amplitude, with lower amplitudes along the edges of the prints as energy there was not being reflected very much from that more vertical interface back to the surface. Radar energy moving downward will tend to reflect away from surfaces that are inclined at an angle, such as those on the edges of the prints. This creates the low amplitudes along the print edges.

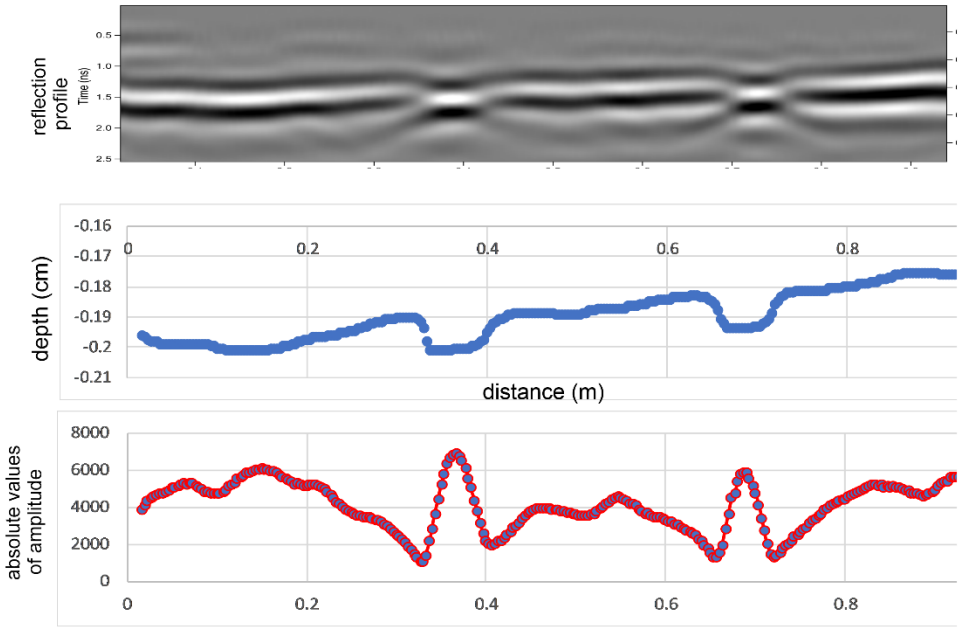

Figure 24: ReflexW data downloaded for file 15 using the 2.6 GHz antenna and plotted for file 15.

All downloaded picked data from all profiles was then put into one Excel spreadsheet to create values for the depth of the clay horizon across the grid. An image of these depths in Figure 25 with blue being "deeper" and red "shallower" shows that the clay horizon was closer to the surface along the edges of my test grid. And there were other anomalous depths that must be related to how I constructed the grid. I had hoped that this map would immediately produce an image of the prints. It did not. Instead it produced a complex surface that had little relationship to the prints that I could see, likely due to how I constructed the test area. When I think more about this, this is not much different than would be expected in the field at Laetoli where an undulating ground surface, and rock layers below the surface that also create similar conditions.

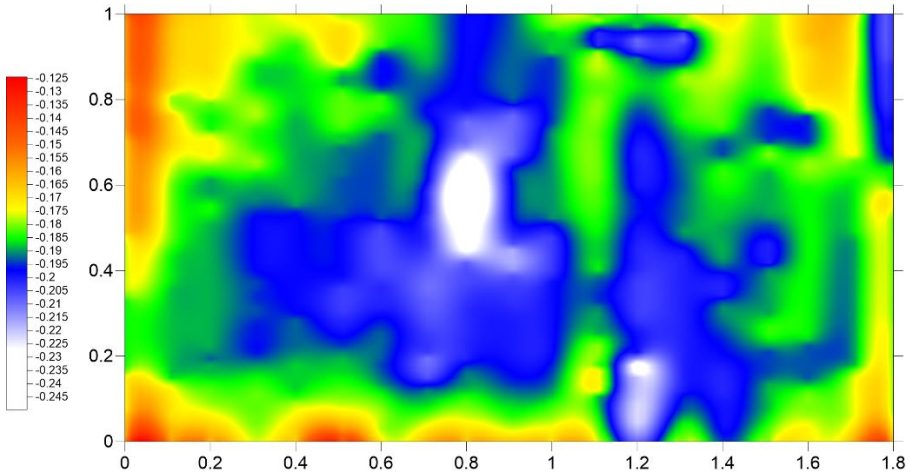

Figure 25: Image map of the depth of the clay horizon below the surface.

In an attempt to create an image of the footprints below the surface I created a topographic map with a .005 cm contour interval (Figure 26). This proved to be much too "busy" but does show a little better some depressions that might be of the prints.

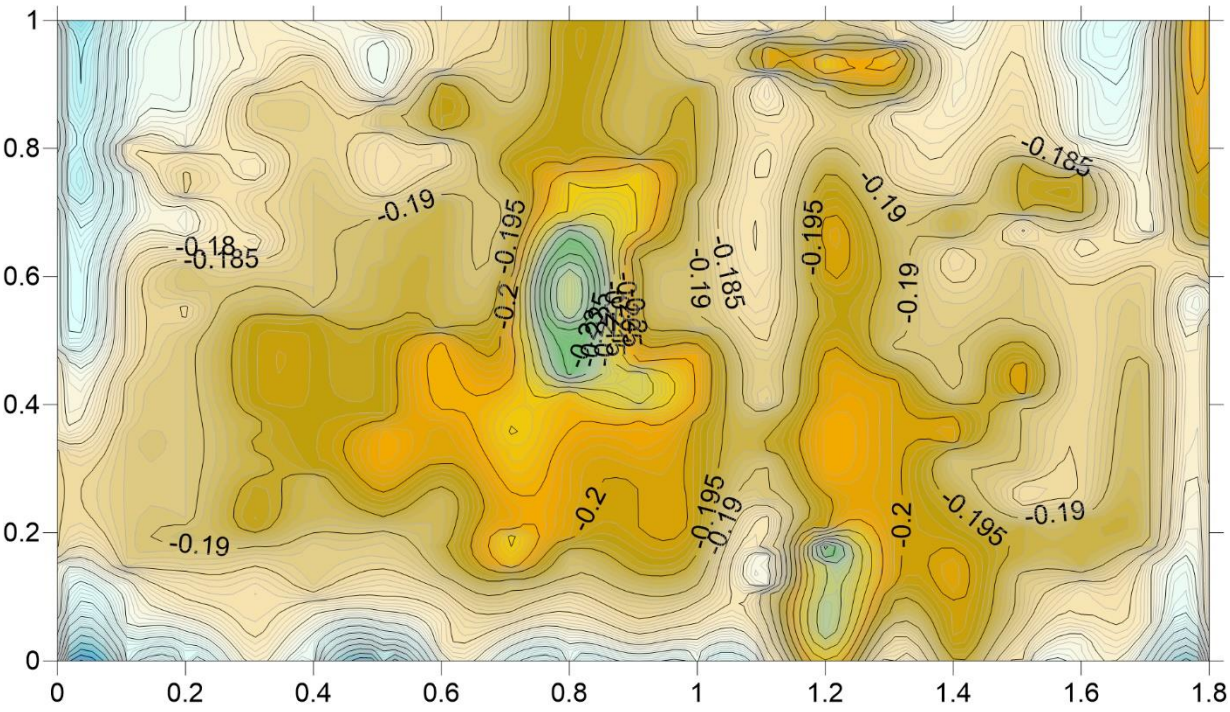

Figure 26: Topographic map of the depth of the clay layer below the top of the yoga mat.

I then visually circled the low depressions on this topographic map which has color on the contour intervals to show the relative low areas (Figure 27).

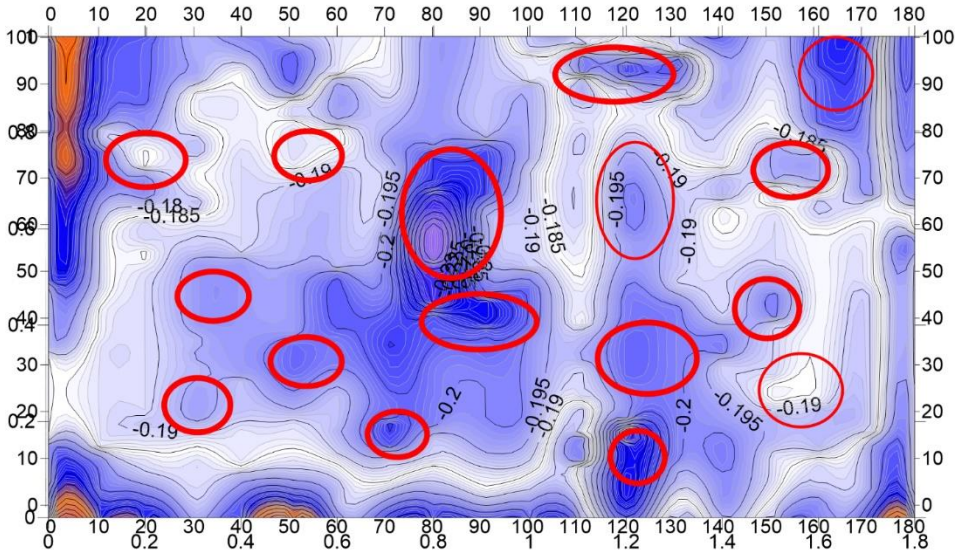

Figure 27: Contour map with red ovals showing the low areas.

When those circled low areas in Figure 27 are placed on top of the image of the prints with the known locations of the prints, there are many correlations, but many more false positives (Figure 28). There are some offsets in the low areas, probably due to antenna wheel slippage or other errors discussed above. But many other variations in the clay surface that are not associated with the prints. There are 4 false positives in this method, which does not give me a great deal of confidence. The error here is likely in the thickness of the sand that was used to cover the prints, and perhaps small errors created by me kneeling on the yoga mat during collection.

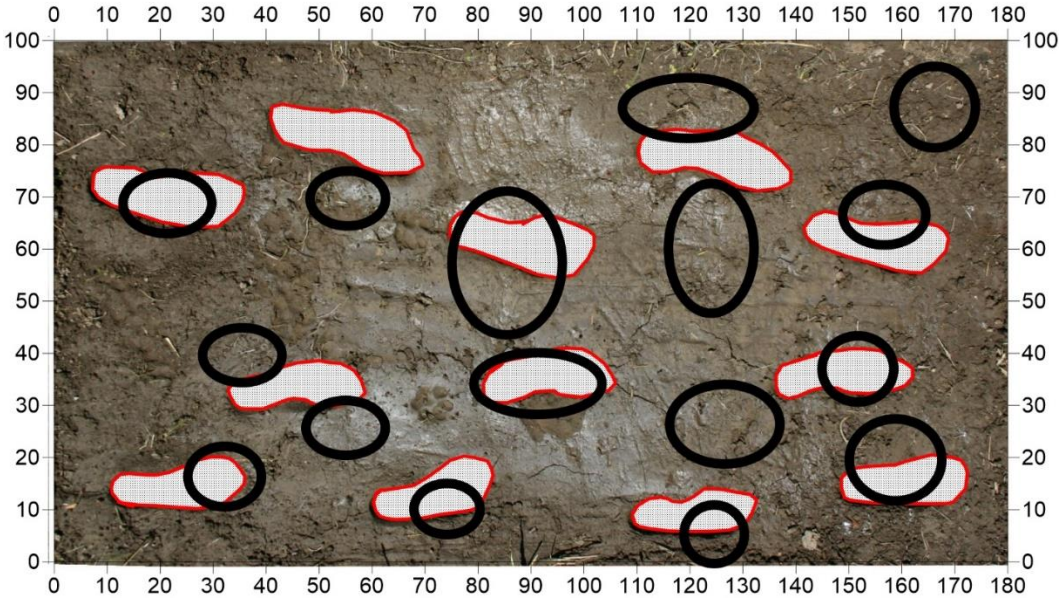

Figure 28: Localized low areas from the topographic map in black with the location of the prints. There are some good correlations, but 4 false positives, making this method less than desirable.

To take out the variations in the clay level and sand thickness I then went through a twostep process to produce a "residual" map of the prints. To do this the depth measurements derived from the ReflexW depth were filtered in Surfer with a Gaussian 3x3 low pass filter and 10 separate passes through the dataset to take out all the minor spatial variations in depth. The contour map produced using this method shows the general depth of this surface, with a 'bowl" shape in the middle, probably due to my construction method (Figure 29). This led me to remember back to my collection using this antenna, and how I had to kneel in the middle of the grid to move the antenna back and forth. That low area in the middle is my kneeling error.

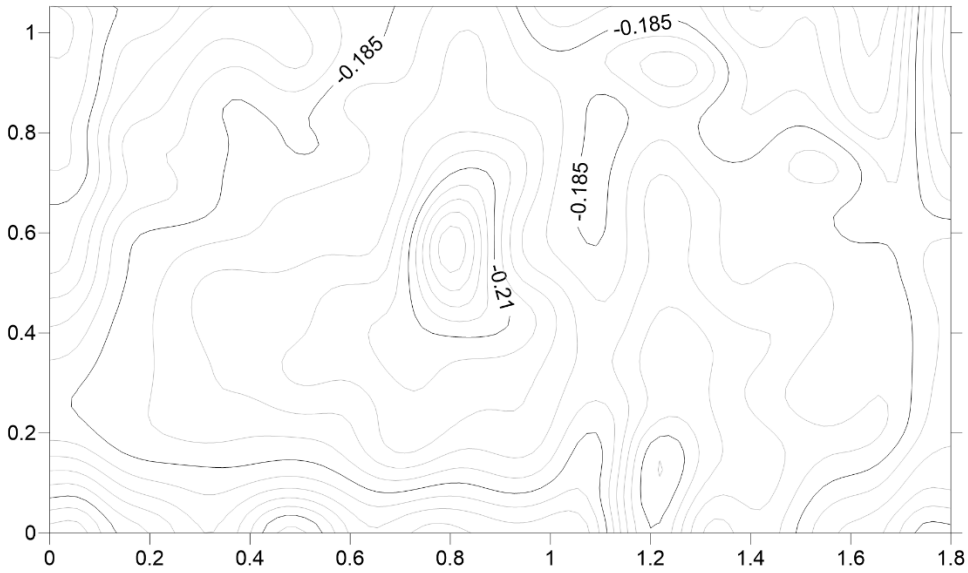

Figure 29: Contour map of the depth to the clay layer, after a low-pass filter was applied to remove many of the smaller scale variations.

The measured depth of the clay from the ReflexW data download was then subtracted from the filtered "general" map to produce a residual map of the clay surface (Figure 30). Here I have colored the low areas in purple, and there is a good correlation between the prints and the low areas. Some false positives are still present, the most prominent being the low area caused by my kneeling on the mat.

After thinking this through a little bit, a way to remove ground surface error at Laetoli would be to make two horizon "picks" from the profiles: one of the top of the lake ash bed where the prints are preserved, and another on a layer above it (but still below the ground surface). A thickness between the base of the overlying unit and the top of the ash layer would then produce a much more accurate location of the prints (this is called an isopach map in geological mapping).

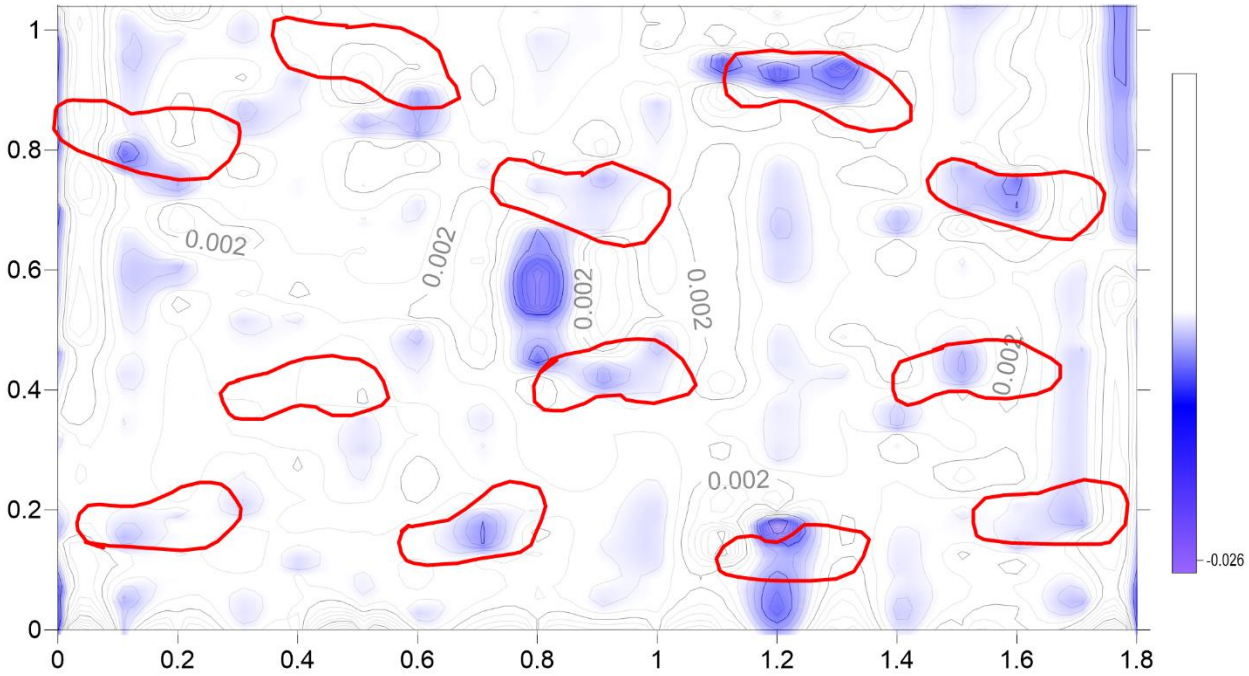

Figure 30: Residual depth map of the top of the clay, produced by subtracting the points in Figure 27 from those in Figure 29.

Another test I did with the 2.6 GHz antenna was a small grid over one very subtle print using a 5 cm profile spacing and 800 traces/meter. The profiles were processed in the same way as the larger grid using GPR Viewer and ReflexW, and the datapoints were then contoured in Surfer (Figure 31). Here the depth and the amplitude of the waves reflected from the clay are shown as images. This is interesting as the depth map shows both the deeper depressions from the heel and the ball of the foot. There is no energy focusing in the middle of the print as is seen in the more pronounced and deeper prints elsewhere. The higher amplitude reflections from the clay adjacent to the print are visible, which is exactly what can be seen in the reflection profiles. This test appears to indicate that by mapping the amplitudes and placing that on the subtle depressions from the less-pronounced prints, there still might be success in very shallow foot depressions.

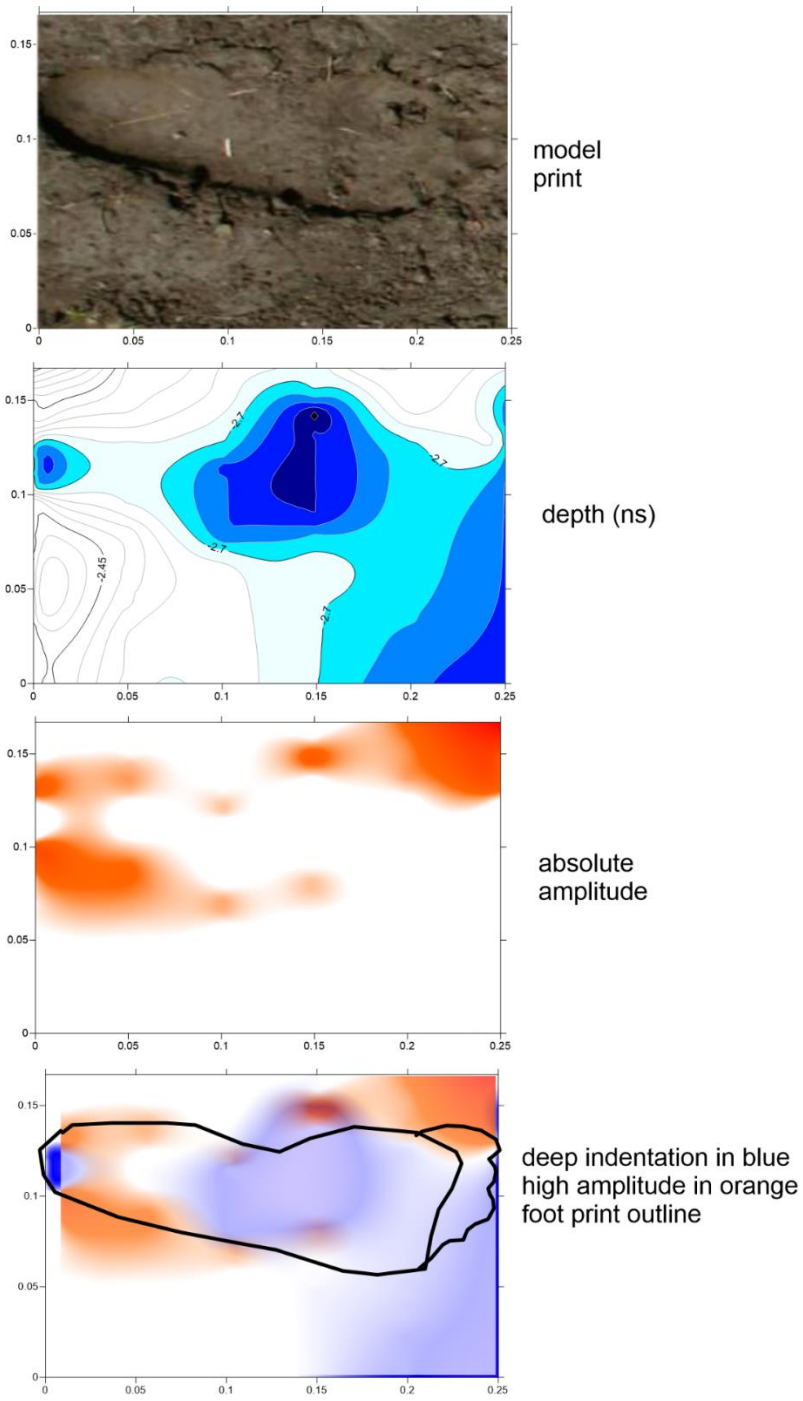

Figure 30: Small grid of 2.6 GHz lines collected over one very shallow print to test resolution potential.

Conclusions

Many errors that I made in the construction of the test bed, and then the collection of the reflection data did not become apparent until I had spent a good deal of time interpreting the results. My kneeling in the middle of the grid to collect produced a much larger error than I had anticipated and was not easily removed from the dataset. Also, slippage of the antenna and some variations in profile length turned out to produce errors in the placement of the reflection features horizontally. This shows how

important it is with high resolution antennas to make certain the start and stop locations of the lines are exact, and that the wheels are firmly on the surface during collection. My first try at using these small antennas has taught me that huge lesson, which the concrete GPR people already learned from experience.

The best processing method that will create "batch results" is the horizon-slicing method where the horizon can be picked, and digital data then exported for mapping in Surfer. This takes some time, as the automatic picking is fraught with errors as the picked layers often skip upward and downward in the waves that are recorded. Editing is necessary for every one of the profiles that are collected. Once these digital data are available, a good deal of image production can be accomplished using standard maps in Surfer. Good results were created using the grid filtering and then the creation of a residual depth map after removing a filtered and average surface contour. This was of great help.

The small test of the 5 cm separated profiles shows how much higher resolution results can be obtained, but with twice the time in data collection. The overlay of the depth and amplitude images in this small grid was encouraging and could be done on a larger grid (such as the 100x180 cm grids I collected).

There was some time spent in manipulation of the data in Excel that needed to be done before the ReflexW downloaded data could be imported into Surfer. That proved tedious, and in the future if many grids are collected in the same way, Excel macros can be employed to conduct the same keyboard steps that took so much time. This would also be the case if several 100x180 cm grids needed to be stitched together to map a much larger area.

The quickest and easiest method for interpretation was the "tried and true" manual interpretation method that I started with (Figures 18 and 21). This method took only about 45 minutes for the whole grid and could be repeated once the methods were perfected. The location results could then be stitched together for many grids that adjoin one another.

The greatest limiting factor for conducting this method in the future on prints that are overlain by various other geological units is depth. The 2.6 GHz antenna here produce energy with a maximum depth penetration of about 25-30 cm. That means that any overburden thicker than that would necessitate a lower frequency antenna to get the radar waves from the surface, to the layer of importance, and back to the surface again to be recorded. Tests here of the 2 GHz were marginally usable for the methods discussed above, but its depth penetration was about the same as the 2.6 GHz. The 900 MHz antenna transmitted radar energy to about 70-80 cm but proved totally inadequate to resolve subtle footprints. It must be remembered that the wavelength of a 2.6 GHz wave is 12.5 cm in air, and once it moves in the ground it becomes shorter. In this ground with a relative dielectric permittivity (RDP) of about 5-7, its transmitted wavelength was about 6 cm. Using the 40% estimate for bed and feature resolution (Conyers 2016), footprints shallower than about 2.5 cm would be invisible. The depth of these prints (and those at Laetoli that are of similar depth) were just at the boundary between being visible and invisible with the 2.6 GHz. This means that in "typical ground" the methods discussed here and using the 2.6 GHz antenna would be impossible to replicate if the print horizon is buried more than about 25 or 30 cm.

Acknowledgements

Many thanks to Peter Leach and Peter Masters of GSSI for kindly lending me their 2.0 and 2.6 GHz antenna. Especially Peter Leach for teaching me on the phone on weekends (while he was taking care of his daughter) some of the tricks needed to calibrate the high frequency antennas.

References cited

Conyers, Lawrence B. and Dean Goodman, 1997: Ground-penetrating radar: An Introduction for Archaeologists. AltaMira Press, Walnut Creek, CA.

Conyers, Lawrence B. 2012: Interpreting Ground-penetrating Radar for Archaeology. Routledge, Taylor and Francis Group, New York

Conyers, Lawrence B. 2016: Ground-penetrating Radar for Geoarchaeology, Wiley-Blackwell Publishers, London.

Conyers, Lawrence B., 2013: Ground-penetrating Radar for Archaeology, Third Edition. Rowman and Littlefield Publishers, Alta Mira Press, Latham, Maryland

Conyers, Lawrence B. 2016: Ground-penetrating radar mapping using multiple processing and interpretation methods: Remote Sensing, v. 8, doi: 10.3990.

Conyers, Lawrence B., Mary-Jean Sutton and Emma St Pierre, E. 2**019:** with Dissecting and Interpreting a Three-Dimensional Ground-Penetrating Radar Dataset: An Example from Northern Australia. *Sensors*, *19*(5), pp. 12-39. doi.org/10.3390/s19051239

Raichlen, D. A., Gordon, A. D., Harcourt-Smith, W. E., Foster, A. D., & Haas Jr, W. R. (2010). Laetoli footprints preserve earliest direct evidence of human-like bipedal biomechanics. *PLoS One*, *5*(3), e9769.